STRUCTURAL INTERPRETATION OF THE BIREFRINGENCE GRADIENT IN RETINAL ROD OUTER SEGMENTS

JOSEPH M. CORLESS, *Departments of Anatomy and Ophthalmology, Duke University Medical Center, Durham, North Carolina 27710*
MICHAEL W. KAPLAN, *Neurological Sciences Institute, Good Samaritan Hospital and Medical Center, Portland, Oregon 97210 U.S.A.*

ABSTRACT The birefringence of frog retinal rod outer segments is analyzed in terms of a three-dielectric layer model. The possibility that the birefringence gradient found in such cells is due to changes in the disk membrane-pair spacing is investigated using previously published glycerol imbibition data (Kaplan et al., 1978. *Biophys. J.* **23**: 59–70). The higher net birefringence of the basal end compared to the midpoint of rod outer segments can be accounted for by a smaller negative form birefringence term due to either a smaller or larger intradiskal space, depending upon the assumed relative solids contents of the intradiskal and cytoplasmic spaces.

INTRODUCTION

Isolated frog rod outer segments (ROSs) often exhibit a nonuniform axial birefringence (Δn) gradient (Liebman, 1975; Kaplan et al., 1978). Within the basal 20–30 μm of the ~50-μm-long outer segments, Δn decreases by $\simeq 2 \times 10^{-5}$ μm^{-1} in the basal-to-distal direction. Within the distal 20–30 μm, Δn is nearly constant. The origins of the Δn gradient have been analyzed by Kaplan et al. (1978) using the technique of glycerol imbibition to separate the positive intrinsic birefringence term, Δn_I, from the negative form birefringence term, Δn_F, where $\Delta n = \Delta n_I + \Delta n_F$. The changes in Δn produced by perfusing ROSs with high refractive index glycerol-containing solutions were interpreted in terms of a system of alternating lamellae of two media having different dielectric constants. From glycerol imbibition curves measured in the basal, middle, and distal regions of ROSs, it was concluded that (*a*) the birefringence gradient in the basal half of the ROSs arises principally from a gradient in the Δn_I component, and (*b*) the Δn_F component is approximately constant along the axis because changes due to increasing membrane refractive index are compensated by a decreasing membrane volume fraction in the basal-to-distal direction.

In this paper we apply a three-dielectric-layer model of ROS substructure to the problem of interpreting the Δn gradient and the glycerol imbibition curves described by Kaplan et al. (1978). It will be shown that when such a model is used, the Δn gradient can be attributed to small differences in the width of the intradisk compartment. No changes in the Δn_I term need be invoked.

One important reason for establishing the physical parameters underlying the Δn gradient is that in all x-ray and neutron-scattering studies to date it has been assumed that the structure of the disk membrane is constant along the ROS axis (Blaurock and Wilkins, 1969

and 1972; Gras and Worthington, 1969; Corless, 1972; Chabre, 1975; Yeager, 1975; Schwartz et al., 1975; Saibil et al., 1976). If the interpretation of the Δn gradient proposed by Kaplan et al. (1978) on the basis of a two-dielectric model is correct, it would be reasonable to conclude that the disk membranes are continually changing structures, especially in the basal portion of the ROS. Such a long-range pattern of systematic substitution disorder would imply that diffraction studies can at best hope to resolve only the main structural features of the membranes, and that detailed profiles are probably unattainable. However, if the Δn gradient is due to a gradient in the Δn_F term, the long-range systematic substitution disorder would be of a significantly different kind, one in which the asymmetric repeating unit changes its relative position but not its structure. For this latter case it is possible, in principle, to desmear the membrane-scattering profiles for such an effect.

METHODS

Rod outer segments contain three components: disk membrane and two aqueous compartments, the intradiskal space and the interdisk cytoplasm. The distribution of the components within the ROS unit cell is schematically depicted in Fig. 1.

This three-layer model is certainly a simplification of the continuous refractive index profile that must be present in the rod outer segment. Interpretations of data in terms of such a model might be considered reasonable approximations.

The form birefringence of a lamellar system composed of three isotropic dielectric layers was derived by Thornburg (1957). In terms of the parameters in Fig. 1,

$$\Delta n_F = \frac{-1}{(n_\parallel + n_\perp)}\left[\frac{d_1 d_2 n_3^2(n_2^2 - n_1^2)^2 + d_2 d_3 n_1^2(n_3^2 - n_2^2)^2 + d_1 d_3 n_2^2(n_1^2 - n_3^2)^2}{d_1 n_2^2 n_3^2 + d_2 n_1^2 n_3^2 + d_3 n_1^2 n_2^2}\right], \quad (1)$$

where $n_\parallel$ and $n_\perp$ are the refractive indices for light linearly polarized parallel to and perpendicular to the ROS axis, d_i is the relative volume fraction and n_i the refractive index of medium i. The value of d_i is computed as the width of medium i within the unit cell, D_i (in Å), divided by 295 Å, the disk-to-disk spacing that is assumed to be constant along the ROS axis. Subscript 1 refers to the intradiskal space, subscript 2 refers to the disk membranes, and subscript 3 refers to the interdiskal cytoplasmic space.

Inasmuch as the term $n_\parallel + n_\perp$ varies slowly with changes in Δn, it is usually replaced by $2n_T$, where n_T is the average ROS bulk refractive index. For purposes of calculating n_T when the ROSs are perfused

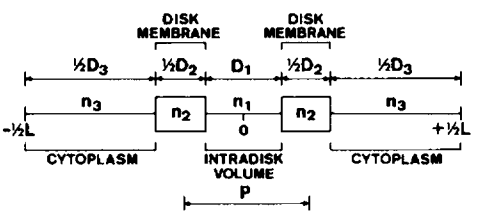

FIGURE 1 Schematic representation of the three-layer dielectric model for the repeating unit of the rod outer segment. The average refractive indices for the intradisk compartment, glycerol-excluding portion of each disk membrane and the cytoplasm are n_1, n_2, and n_3, respectively. The glycerol-excluding width of each membrane is $\frac{1}{2} D_2$. The axial repeat period of the disks is L. The volume fraction for each layer of the model is D_i/L. The center-to-center membrane pair spacing is P, the range of values for which is inferred from x-ray scattering data.

with saline or glycerol-saline solutions, we assume that

$$n_T = (d_1 n_1^2 + d_2 n_2^2 + d_3 n_3^2)^{1/2}. \tag{2}$$

Values of n_1 and n_3 depend upon the refractive index of the imbibing perfusate, n_p, and the solids concentrations (grams/100 ml), s_1 and s_3, as given by (Sidman, 1957):

$$n_i = n_p + 0.0018\, s_i. \tag{3}$$

The membrane refractive index, n_2, is assumed to be independent of n_p. The value of n_T for frog ROS in water saline solutions ($n_p = 1.335$) is $\simeq 1.41$ (Sidman, 1957; Blaurock and Wilkins, 1969; Enoch et al., 1973). Sidman's value of $n_T = 1.4106$ is used in our calculations.

Plots of Δn as a function of n_p using the three-dielectric ROS model have several properties not seen in the two-dielectric model:

(*a*) If n_1 does not equal n_3, Δn_F never becomes zero by perfusing the ROS with high refractive index media. As a consequence, Δn_i cannot be assigned from the peak value of the imbibition curve. Only a minimum value for Δn_i can be deduced.

(*b*) The form component of birefringence, Δn_F, will change as the fractional volumes of the intra- and interdisk compartments change. Thus, for a given lamellar repeat period and a given membrane volume fraction, one predicts changes in Δn_F if the width of the intradisk compartment changes. The effect can be outlined as follows. When a disk membrane pinches off from the plasma membrane, solids sequestered initially within the disk are assumed to be retained in the intradiskal space as the disk is displaced along the ROS axis by the disk renewal process (Young, 1967; Besharse et al., 1977*a*). If the disk swells or shrinks due to movement of water and small ions, the consequent change in composition of the intradiskal and cytoplasmic spaces will affect n_1 and n_3. These changes in volume fractions and refractive indices will change Δn_F (Eq. 1).

New values, n_1' and n_3', can be calculated by assuming a uniform redistribution of solids so that

$$n_i' = 1.335 + (n_i - 1.335)\,(d_i \pm \Delta d)/d_i, \tag{4}$$

where Δd is the change in volume fraction for medium i. Alternatively, n_1 and n_3 can be calculated by assuming that the dielectric constants of the initial medium and the added or subtracted water sum linearly so that

$$n_i' = \{[d_i n_i^2 \pm (1.335)^2 \Delta d]/(d_i \pm \Delta d)\}^{1/2}. \tag{5}$$

For reasonable values of n_1, n_3, d_1, d_3, and Δd, the two methods yield nearly identical values for n_1', n_3', and n_T.

The procedure for evaluating ROS birefringence gradients in terms of altered membrane-pair spacing[1] using a three-dielectric model is as follows.

(*a*) A value for $(\Delta n_i)_{\min}$ is assigned using the maximum value observed for the glycerol imbibition curve. In the example cell described by Tables I and II this value is 0.00406 ± 0.00019, the highest measured Δn for the basal point. So we set $(\Delta n_i)_{\min} = 0.00387$. For purposes of evaluating the changing membrane-pair spacing hypothesis, we assume that this value is constant along the ROS axis.

(*b*) The disk-to-disk repeat distance (unit cell) is assumed to be constant. From x-ray diffraction data, this distance is assigned a value of 295 Å (Blaurock and Wilkins, 1969; Corless, 1972).

(*c*) Values of Δn for the different experimental values of n_p are calculated using a series of values for n_i and d_i. The independent variables are d_1, d_2, n_1, and n_2. Dependent variables are $d_3 = 1 - d_1 - d_2$; Δn_i and $n_3 = \{[(1.4106)^2 - d_1 n_1^2 - d_2 n_2^2]/d_3\}^{1/2}$. For each set ($i$) of model parameters, the calculated $\Delta n_F(i)$ (negative) is added to the corresponding experimentally derived Δn, to give a computed $\Delta n_i(i)$. If

[1]The membrane-pair spacing of a disk, P, designates the distance between the centers of the two disk membranes. A change in the membrane-pair spacing, ΔD, would be associated with a change of ΔD in the width of the intradisk compartment.

TABLE I

BIREFRINGENCE DATA FROM SINGLE FROG ROS AT DIFFERENT POINTS ALONG ITS LENGTH*

Refractive index of imbibing Ringer solution	Basal point		Mid-point		Distal point	
	Δn‡	Error	Δn‡	Error	Δn‡	Error
1.335	0.00017	0.00013	−0.00047	0.00004	−0.00059	0.00006
1.348	0.00080	0.00006	0.00019	0.00005	0.00021	0.00004
1.361	0.00157	0.00012	0.00087	0.00006	0.00073	0.00004
1.386	0.00253	0.00015	0.00189	0.00008	0.00186	0.00008
1.418	0.00352	0.00018	0.00309	0.00015	0.00293	0.00013
1.445	0.00406	0.00019	0.00365	0.00019	0.00346	0.00019
1.463	0.00396	0.00021	0.00342	0.00017	0.00348	0.00016

*Fixation and mounting details are given by Kaplan et al. (1978). This ROS, 7 μm in diameter, was obtained from a retina fixed 15 min in 2.5% glutaraldehyde in Ringer solution (Kaplan and Liebman, 1977). After mounting, the rod was totally bleached and allowed to equilibrate for 20 min before data collection.

‡Mean value based upon five or more measurements.

this computed $\Delta n_l(i)$ is less than the experimentally observed $(\Delta n_l)_{\min}$, the set of parameters is discarded. If the computed $\Delta n_l(i)$ is equal to or greater than $(\Delta n_l)_{\min}$, then for each experimental value of $n_p(j)$ we compute a value for the net birefringence, $\Delta n_{\text{calc}}(i, j)$. The quality of fit between the observed and calculated net birefringence is measured as the sum

$$\text{LSQ}(i) = \sum_{j=1}^{7} (\Delta n_{\text{calc}}(i,j) - \Delta n(j))^2. \tag{6}$$

As the calculations proceed and successive models are evaluated, an updated listing of the models that yield the 10 lowest values of LSQ (i) is retained. The 10 models that best fit the experimental imbibition data for the midpoint of the ROS are thus obtained.

The regions of parameter space to be explored were constrained in the following way. Reasonable limits for the dimensions of the dielectric lamellae are determined from x-ray diffraction studies. In isosmotic solutions the membrane-pair spacing, P, is ≃90 Å (Blaurock and Wilkins, 1969 and 1972; Corless, 1972; Chabre, 1975). The minimum P observed in hyperosmotic media is ≃73 Å; the maximum P observed in hypo-osmotic media is ≃102 Å. We therefore assume a range of 73 Å $\leq P \leq$ 102 Å in our calculations. The width of each disk membrane is varied from 30 (0.22 × 295 Å/2, Kaplan et al., 1978) to 50 Å, a reasonable maximum width for the high refractive index, glycerol-excluding region of the membrane. We have evaluated 2 Å $\leq D_1 \leq$ 72 Å and 30 $\leq 1/2\, D_2 \leq$ 50 Å. Limits chosen for the refractive indices were 1.335 $\leq n_1 \leq$ 1.435 and 1.448 $\leq n_2 \leq$ 1.520 (Table III).

In Table III, as well as in Tables V and VII all possible combinations of parameters were evaluated.

(d) Once the 10 best fit values for different sets of n_i and d_i are found for the ROS midpoint, the

TABLE II

OPTIMAL PARAMETERS DERIVED FROM A TWO-LAYER DIELECTRIC MODEL FOR FORM BIREFRINGENCE (n_T = 1.4106)

Parameter	Basal point	Mid-point	Distal point
d_2	0.22	0.23	0.20
$\frac{1}{2}D_2$	32.5 Å	33.9 Å	29.5 Å
n_2	1.511	1.511	1.521
Δn_l	0.0040	0.0036	0.0036
C_s*	26	25	26

*Average bulk concentration of solids in aqueous compartments (grams/100 cm^3).

TABLE III

INITIAL RANGES OF PARAMETERS USED TO EVALUATE THE ROS MID-POINT BIREFRINGENCE DATA IN TERMS OF A THREE-LAYER DIELECTRIC MODEL FOR FORM BIREFRINGENCE*

Parameter	Minimum value	Maximum value	Increment
n_1	1.335	1.435	0.01
n_2	1.448	1.520	0.006
$^1/_2D_2$	30	50	2
D_1	2	$102-{}^1/_2D_2$	4

*Bulk-refractive index of ROS assumed constant, with $n_T = 1.4106$. A constant lamellar repeat, $L = 295$ Å, is also assumed. The dependent variables, Δn_f, d_3, and n_3, are derived from the above parameters as outlined in the text.

membrane pair-spacing of the disk is changed (Eq. 5), and the recomputed values of Δn as a function of n_p are compared to the imbibition data measured at the basal point. If the recomputed values closely match the experimental basal point imbibition data, the result is interpreted to mean that the birefringence gradient can be accounted for as a change in Δn_F due to changes in the membrane-pair spacing for that particular set of initial n_i and d_i.

The results reported herein are based on birefringence data obtained from a single frog ROS. This set of data is representative of the data obtained by Kaplan et al. (1978) in their studies of the birefringence gradient in frog ROSs, and was presented in their Fig. 3. We feel that such a representative set of data is entirely adequate for the present investigation.

The computer modeling studies were carried out on a TP-5000 Computer System (Tennecomp Systems, Inc., Oak Ridge, Tenn.), which uses a PDP 11/05 (Digital Equipment Corp., Marlboro, Mass.) as the central processor. Graphic output is provided by a Tektronix 4012 terminal equipped with hard copy unit (Tektronix, Inc., Beaverton, Oreg.).

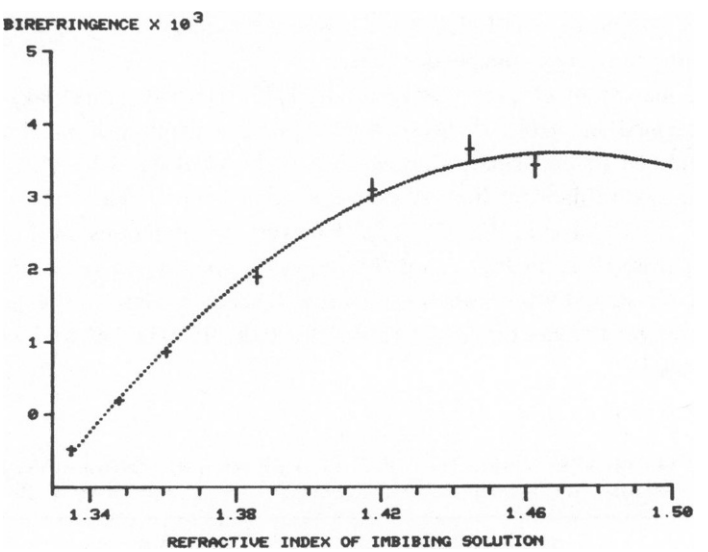

FIGURE 2 Computed imbibition curves of the 10 initial models for the mid-point birefringence data (Table IV). The 10 curves are virtually identical and cannot be distinguished in this figure. The ROS mid-point birefringence data, plotted as $\Delta n \pm$ error vs. n_p (Table I), are superimposed. The width of the horizontal line in each data point has no statistical significance; this line only identifies the average value of Δn from the measurements.

TABLE IV

10 BEST-FIT MODELS OF ROS MID-POINT BIREFRINGENCE DATA FOR THE RANGES OF PARAMETERS LISTED IN TABLE III

Model	D_1	$\frac{1}{2}D_2$	D_3	n_1	n_2	n_3	Δn_f
1	66	32	165	1.415	1.514	1.3666	0.00409
2	58	32	173	1.345	1.514	1.3923	0.00404
3	62	32	169	1.345	1.514	1.3934	0.00408
4	62	32	169	1.415	1.514	1.3677	0.00404
5	42	32	189	1.335	1.514	1.3905	0.00408
6	38	32	193	1.335	1.514	1.3894	0.00402
7	46	32	185	1.425	1.514	1.3693	0.00410
8	42	32	189	1.425	1.514	1.3705	0.00404
9	30	32	201	1.435	1.514	1.3723	0.00404
10	34	32	197	1.435	1.514	1.3710	0.00412

RESULTS

The initial 10 sets of model parameters that gave the best least-square fits for the Δn data obtained from the ROS midpoint are summarized in Table IV. The 10 corresponding imbibition curves are shown in Fig. 2. The 10 curves are virtually identical, and are not distinguishable. Two important observations should be noted in Table IV. The membrane width, $D_2/2$, and refractive index of the glycerol-excluding region of the membrane, n_2, are the same in all 10 models. In fact, very similar values are obtained if a two-dielectric ROS model is used to analyze the data (Table II). From these observations we infer that the membrane width and refractive index are well approximated by the values obtained. Table IV contains models in which the intradiskal bulk refractive index, n_1, is either higher or lower than that of the cytoplasm, n_3. Models 3 and 4 emphasize this point. The choice between such models will require ancillary, independent data.

Because the increment of each parameter in Table III was rather large, the ranges of parameters obtained in Table IV were used to more narrowly limit the range of each parameter examined so that smaller increments could be evaluated. The parameter values examined in the next refinement step are summarized in Table V. The 10 best least-square fits are shown in Table VI and Fig. 3. The 10 overlapping curves in Fig. 3 are hardly distinguishable from those in Fig. 2. Furthermore, the membrane refractive index, n_2, and width, $D_2/2$, are essentially the same for all fits and are very close to the values obtained in Table IV. The range of values for Δn_f in Table VI is 0.00395–0.00447, and includes the range observed in Table IV.

TABLE V

RANGES OF PARAMETERS USED TO FURTHER REFINE THE THREE-LAYER DIELECTRIC MODEL BASED UPON THE SURVEY RESULTS IN TABLE IV

Parameter	Minimum value	Maximum value	Increment
n_1	1.335	1.435	0.005
n_2	1.500	1.520	0.001
$\frac{1}{2}D_2$	28	36	1
D_1	26	70	2

TABLE VI

10 BEST-FIT MODELS OF ROS MID-POINT BIREFRINGENCE DATA FOR THE RANGES OF PARAMETERS LISTED IN TABLE V

Model	D_1	$\frac{1}{2}D_2$	D_3	n_1	n_2	n_3	Δn_f
1	52	33	177	1.435	1.511	1.3638	0.00447
2	52	33	177	1.415	1.512	1.3695	0.00395
3	36	33	193	1.425	1.512	1.3714	0.00396
4	60	33	169	1.430	1.511	1.3622	0.00447
5	30	33	199	1.430	1.512	1.3723	0.00396
6	34	33	195	1.335	1.512	1.3877	0.00395
7	54	33	175	1.415	1.512	1.3690	0.00397
8	44	33	185	1.420	1.512	1.3703	0.00397
9	52	33	177	1.345	1.512	1.3901	0.00395
10	66	33	163	1.335	1.511	1.3982	0.00444

Each set of parameters in Table VI was then examined to see if the glycerol imbibition data obtained from the basal ROS could be modeled by simply increasing D_1 and decreasing D_3, as outlined earlier. Fig. 4 shows the imbibition curves derived from model 1 of Table VI, in which D_1 is increased in steps of 4 Å. The trend is obvious. As D_1 increases, the imbibition curve is shifted upward. Similar results are obtained using model 4. However, for models 2, 3, 5, 7, and 8 the upward shift of the imbibition curve with increasing D_1 reaches a limiting value before intersecting the observed imbibition data points for the basal end of the ROS, and as D_1 is further increased the computed curves are progressively lowered. For models 6, 9, and 10 the imbibition curve is shifted downward by increasing D_1. In these three models the refractive index of the medium within the disk is low ($1.335 \leq n_1 \leq 1.345$). In models 2, 3, 5, 7, and 8 the values for n_1 are higher ($1.415 \leq n_1 \leq 1.430$), but Δn_f is low ($\Delta n_f \simeq 0.00396$). In models

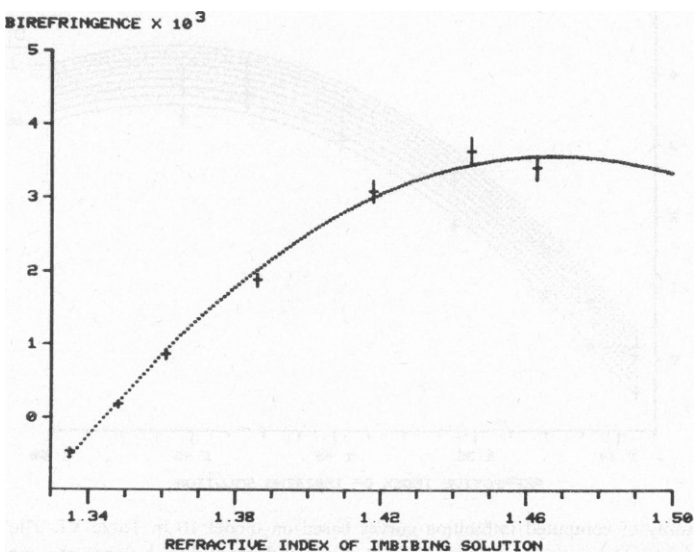

FIGURE 3 Computed imbibition curves of the 10 models for the mid-point birefringence data listed in Table VI. All 10 curves are again practically identical.

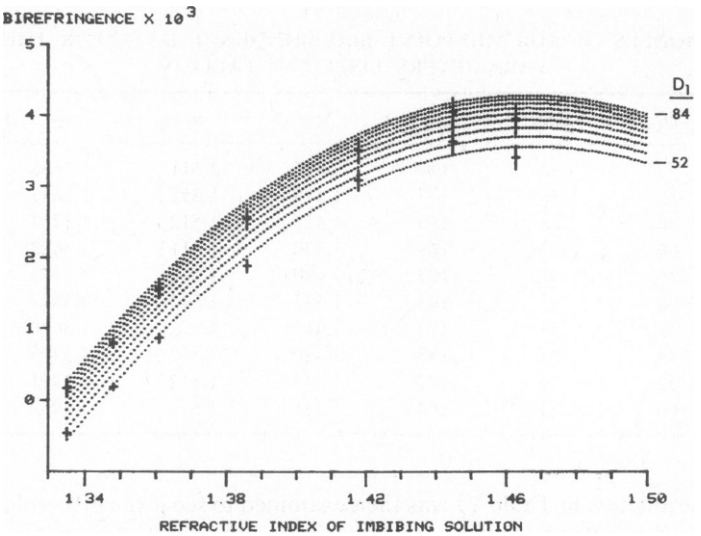

FIGURE 4 Family of computed imbibition curves based on model 1 in Table VI. The lowest curve is computed for model 1 and is contained within the curves plotted in Fig. 3. As D_1 is increased (4 Å steps), the imbibition curves shift upward. After increasing D_1 by 20 Å, the associated imbibition curve fits the basal point birefringence data rather well. The lower set of data points represents the mid-point Δn measurements; the upper set, the basal Δn values. In these computations, the values for D_2, n_2, n_T, L, and Δn_f are kept constant.

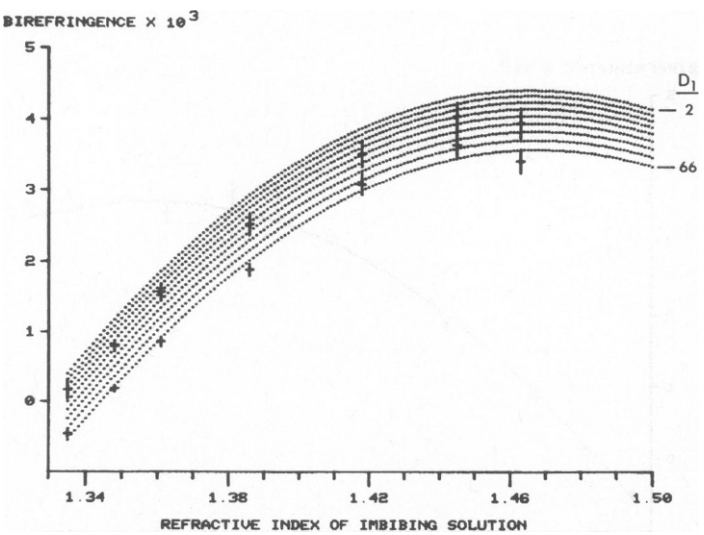

FIGURE 5 Family of computed imbibition curves based on model 10 in Table VI. The lowest curve represents model 10, and is also contained in Fig. 3. As D_1 is decreased (8 Å steps), the imbibition curves shift upward.

TABLE VII

RANGES OF PARAMETERS USED TO OPTIMIZE THE THREE-LAYER DIELECTRIC MODEL OF FORM BIREFRINGENCE FOR BOTH THE BASAL AND MID-POINT ROS BIREFRINGENCE DATA*

Parameter	Minimum value	Maximum value	Increment
D_1	28	68	2
n_1	1.415	1.455	0.002
ΔD	10	60	2

*The following values were used in all calculations: $n_T = 1.4106$; $n_2 = 1.511$; $\frac{1}{2}D_2 = 33$.

1 and 4, n_1 and Δn_I are both large. Hence, we conclude that the Δn gradient observed in frog ROSs can be explained as a form birefringence effect arising from a narrower intradisk space at the midpoint than at the basal end, when the intrinsic birefringence and intradiskal solids content are assigned relatively high values. The differences in width between the intradisk space at the midpoint and basal regions of the rod is designated ΔD.

We have also investigated the effects of decreasing the width of the intradisk space on the computed midpoint imbibition curve for the models listed in Table VI. Only model 10 can account for the Δn gradient. The family of computed imbibition curves obtained by decreasing the membrane-pair spacing[1] is shown in Fig. 5.

To choose between an increasing or a decreasing membrane-pair spacing as the more likely explanation for the Δn gradient (assuming one or the other is the source), additional independent data are needed. For reasons given in the Discussion section, we favor the notion that the intradiskal volume decreases as a function of distance from the base of the ROS.

Finally, we have optimized the form birefringence models in two ways. The 10 best least-squares fits for the midpoint Δn data are chosen from the parameter ranges in Table VII. Then for each of these choices we search for the increase in the width of the intradisk space, ΔD, that best accounts for the basal point imbibition curve. The results are shown in Table VIII and Fig. 6. In a second procedure, we seek values for n_1, D_1, and ΔD for which the sum of errors of the models chosen for both the midpoint and basal point Δn data is

TABLE VIII

10 BEST-FIT MODELS OF ROS MID-POINT BIREFRINGENCE DATA FOR THE RANGES OF PARAMETERS LISTED IN TABLE VII, AND THE VALUE OF ΔD FOR EACH MODEL THAT GIVES THE BEST FIT FOR THE BASAL BIREFRINGENCE DATA

Model	D_1	D_3	n_1	n_3	Δn_I	ΔD
1	40	189	1.445	1.3662	0.00447	18
2	52	177	1.435	1.3638	0.00447	20
3	58	171	1.431	1.3627	0.00447	22
4	38	191	1.447	1.3667	0.00446	16
5	62	167	1.429	1.3618	0.00448	22
6	32	197	1.455	1.3678	0.00448	14
7	44	185	1.441	1.3655	0.00446	18
8	42	187	1.443	1.3658	0.00447	18
9	66	163	1.427	1.3609	0.00448	22
10	50	179	1.437	1.3641	0.00449	18

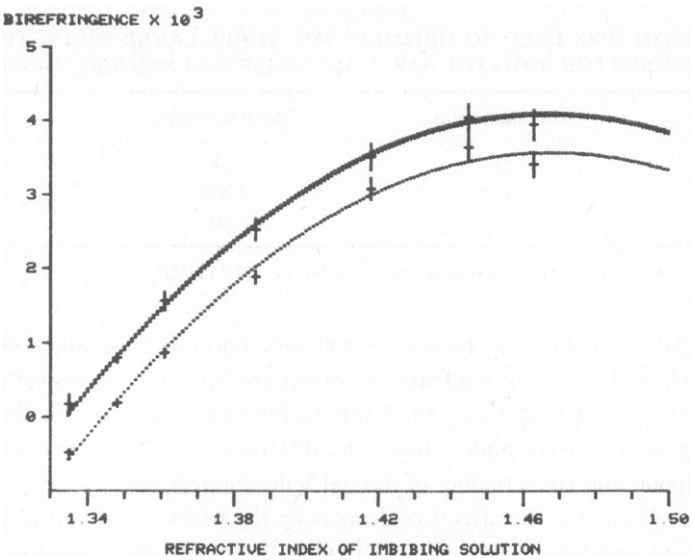

FIGURE 6 Imbibition curves plotted for the models listed in Table VIII. First, the 10 best fits for the mid-point Δn data were determined. Then, for each model the value of ΔD that produced the best fit to the basal Δn data was determined.

minimized. For each model of the midpoint Δn data in Table VII, we search for the value of ΔD producing the best fit for the basal point data; Σ = (sum of errors for the midpoint curve fit) + (sum of errors for the basal curve fit). The mid-point values for n_1, D_1, and the value for ΔD which yield the 10 smallest values for Σ are given in Table IX. The corresponding curves are plotted in Fig. 7.

DISCUSSION

Potential Sources of the Δn Gradient

We have shown that the birefringence gradient observed in frog ROSs can be accounted for in terms of form birefringence effects that arise from a systematic change in the disk membrane-pair spacing as a function of distance along the ROS axis when the ROS is modeled as a composite body having lamellae of three different dielectric constants. As shown in Figs. 4 and 5, both increasing and decreasing the intradiskal volume can produce the Δn gradient, depending upon the relative concentration of solids in the intradiskal and cytoplasmic compartments.

It can be argued that the intradiskal volume decreases as a function of distance from the base of the outer segment. Kaplan et al. (1978) occasionally noticed a highly birefringent band ($\Delta n \simeq 0.0040$) $\sim$ 2 μm wide at the extreme basal end of the ROS. Besharse et al. (1977*a*) showed that in *Xenopus laevis* tadpoles the newly forming disks at the basal end of the ROS are characterized by a rather large intradiskal space compared to disks located more distally. If the highly birefringent band noted by Kaplan et al. (1978) corresponds to a region of open disks, such as those reported by Besharse et al. (1977*a*), then we would conclude that the intradiskal volume decreases as the disks move distally. This hypothesis corresponds to the

TABLE IX

10 BEST-FIT MODELS OF ROS MID-POINT AND BASAL BIREFRINGENCE DATA FOR THE RANGES OF PARAMETERS LISTED IN TABLE VII, FOR WHICH THE SUM OF LEAST-SQUARE ERRORS OF THE MID-POINT AND BASAL MODELS ARE MINIMAL*

Model	D_1	D_3	n_1	n_3	Δn_f	ΔD
1	44	185	1.427	1.3690	0.00407	48
2	34	195	1.435	1.3705	0.00407	42
3	64	165	1.417	1.3658	0.00408	46
4	68	161	1.415	1.3654	0.00407	54
5	32	197	1.437	1.3709	0.00407	42
6	48	181	1.425	1.3682	0.00409	58
7	42	187	1.429	1.3691	0.00409	38
8	60	169	1.419	1.3663	0.00409	42
9	36	193	1.433	1.3703	0.00407	44
10	54	175	1.421	1.3675	0.00407	50

*For all models, $\frac{1}{2}D_2 = 33$ and $n_2 = 1.511$.

calculations plotted in Fig. 4 in which larger intradiskal volumes are associated with higher values of Δn.

A corollary conclusion to be drawn from the above model of the Δn gradient is that the refractive index of the medium within the disks, n_1, is greater than that of the cytoplasm, n_3, based upon the evaluation and discussion of Table VI. Further discussion is given by Corless (1979).

Estimates for the total change in width of the intradiskal space over the length of the Δn gradient, ΔD, can be found in Tables VIII and IX. Two trends are evident. In Table VIII the range of values for ΔD is 14 Å to 22 Å, the intrinsic birefringence is $\simeq$0.00447 and the average value of n_1 is 1.439. In Table IX the values of ΔD are larger (38–58 Å), the intrinsic

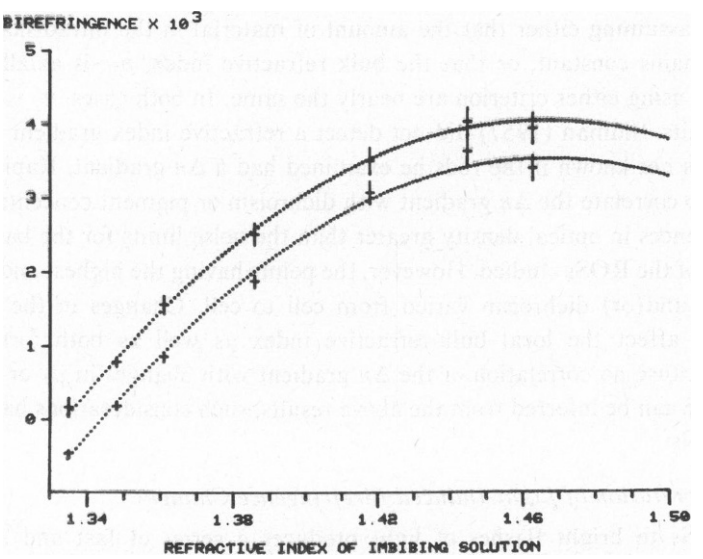

FIGURE 7 Imbibition curves plotted for the models listed in Table IX.

birefringence is lower ($\Delta n_f = 0.00408$), and the average value of n_1 is somewhat lower ($\bar{n}_1 = 1.426$). The corresponding curves for these models in Figs. 6 and 7 all show very good fits to the data. Accordingly, it is not possible to reasonably select the model most likely to be correct. Hence, the value of ΔD cannot be conclusively assigned. The striking effect of small values of ΔD on the scattered x-ray intensities from ROSs has been previously demonstrated (Corless, 1972).

The models in Tables VIII and IX have been examined to see which could account for the bright birefringent band at the base of the ROS discussed earlier. For none of the models in Table IX could the birefringence be significantly increased by increasing ΔD. The main reason for this result is the rather low value of Δn_f. In contrast, all models in Table VIII show obvious increases in net Δn with further increases in ΔD, although the high value of $\Delta n \simeq 0.0040$ cannot be obtained by this method.

The Assumption of Constant Disk-to-Disk Spacing and Constant n_T Along the ROS

In the above modeling studies we have assumed that the disk-to-disk repeat period is constant along the ROS axis. However, there is independent evidence that such might not be the case. Besharse et al. (1977*b*) have followed the axial movement of radioactively labeled bands of disks as a function of time after injecting tritiated leucine. In *Rana pipiens* tadpoles exposed to light for 12 h/day, the average rate of band displacement was 1 μm/day between days 1 and 7, and 0.63 μm/day thereafter. This change in the rate of displacement occurs when the band is located $\simeq$ 8 μm from the base of the rod, a distance representing $\simeq$ 1/3 of the 25-μm length of tadpole ROSs. Inasmuch as the daily rate of disk synthesis appears to proceed at a constant rate at the base of the ROS, the decrease in the mean rate of band displacement distally indicates a decreasing disk-to-disk lamellar repeat distance. It is not known if the rate of band displacement during days 1–7 is constant or exhibits a gradient.

As mentioned previously, the changes produced in n_1 and n_3 by changing d_1 and d_3 can be calculated by assuming either that the amount of material in the intradiskal space and the cytoplasm remains constant, or that the bulk refractive index, n_T, is axially uniform. The values derived using either criterion are nearly the same. In both cases, n_T is constant within observable limits. Sidman (1957) did not detect a refractive index gradient in the ROSs he examined. It is not known if the rods he examined had a Δn gradient. Kaplan et al. (1978) were unable to correlate the Δn gradient with dichroism or pigment concentration. They did observe differences in optical density greater than the noise limits for the basal, middle, and distal regions of the ROSs studied. However, the points having the highest and lowest pigment concentration and(or) dichroism varied from cell to cell. Changes in the lamellar repeat period should affect the local bulk-refractive index as well as both form and intrinsic dichroism. Because no correlation of the Δn gradient with changes in n_T or the disk-to-disk repeat distance can be inferred from the above results, such considerations have been omitted from the models.

Interpretation of Light-Induced Birefringence Changes

Exposing ROSs to bright flashes of light produces a series of fast and slow changes in birefringence (Liebman et al., 1974; Kaplan and Liebman, 1977). In view of the above

reinterpretation of the ROS Δn gradient using a three-dielectric layer model, the relative contributions of changes in the intrinsic and form birefringence components to the light-induced changes in net Δn should be reexamined. For example, Uhl et al. (1977) have concluded that the fast light-induced light-scattering transient recorded from bovine ROS fragments arises from a rapid reduction of intradisk volume. Such a volume reduction must be associated with a change in the form birefringence of the system. A more complete theoretical and experimental analysis of the light-induced birefringence changes using a three-dielectric ROS model is in preparation.

In conclusion, we have shown that the birefringence gradient observed in frog ROSs can be accounted for by a gradient in the form birefringence component due to a changing membrane-pair spacing. However, this analysis has not eliminated the possibility that the gradient arises from an intrinsic birefringence component or that changes in disk-to-disk spacing are associated with the gradient. Furthermore, the lateral shift of the distal point imbibition curve relative to the basal point curve, attributed to an increasing membrane-refractive index by Kaplan et al. (1978), cannot be simulated by a simple change of membrane-pair spacing. A conclusive interpretation of the birefringence gradient will require additional information regarding the ROS component-refractive indices, the membrane-pair spacing and the disk-to-disk spacing along the ROS axis. A precise understanding of the birefringence gradient would seem to be an essential prerequisite for the analysis of high-resolution x-ray and neutron-scattering data from rod outer segments.

We would like to thank C. D. B. Bridges, E. A. Dratz, P. A. Liebman, and J. G. Hollyfield for helpful discussions.

This work was supported by U.S. Public Health Service grant EY01659 and Research Career Development Award EY00016 to Dr. Corless, and by U.S. Public Health Service grant EY01779 and grants from the Oregon Lions Sight Foundation to Dr. Kaplan.

Received for publication 6 September 1978 and in revised form 18 December 1978.

REFERENCES

BESHARSE, J. C., J. G. HOLLYFIELD, and M. E. RAYBORN. 1977*a*. Turnover of rod photoreceptor outer segments. II. Membrane addition and loss in relationship to light. *J. Cell Biol.* **75**:507–527.

BESHARSE, J. C., J. G. HOLLYFIELD, and M. E. RAYBORN. 1977*b*. Photoreceptor outer segments: accelerated membrane renewal in rods after exposure to light. *Science (Wash. D.C.).* **196**:536–538.

BLAUROCK, A. E., and M. H. F. WILKINS. 1969. Structure of frog photoreceptor membranes. *Nature (Lond.).* **223**:906–909.

BLAUROCK, A. E., and M. H. F. WILKINS. 1972. Structure of retinal photoreceptor membranes. *Nature (Lond.).* **236**:313–314.

CHABRE, M. 1975. X-ray diffraction studies on retinal rods. I. Structure of the disc membrane, effect of illumination. *Biochim. Biophys. Acta.* **382**:322–335.

CORLESS, J. M. 1972. Lamellar structure of bleached and unbleached rod photoreceptor membranes. *Nature (Lond.).* **237**:229–231.

CORLESS, J. M. 1979. The carbohydrates in frog retinal rod outer segments. *Prog. Histochem. Cytochem.* In press.

ENOCH, J. M., J. SCANDRETT, and F. L. TOBEY, JR. 1973. A study of the effects of bleaching on the width and index of refraction of frog rod outer segments. *Vision Res.* **13**:171–183.

GRAS, W. J., and C. R. WORTHINGTON. 1969. X-ray analysis of retinal photoreceptors. *Proc. Natl. Acad. Sci. U.S.A.* **63**:233–238.

KAPLAN, M. W., M. E. DEFFEBACH, and P. A. LIEBMAN. 1978. Birefringence measurements of structural inhomogeneities in *Rana pipiens* rod outer segments. *Biophys. J.* **23**:59–70.

KAPLAN, M. W., and P. A. LIEBMAN. 1977. Slow bleach-induced birefringence changes in rod outer segments. *J. Physiol. (Lond.)*. **265**:657–672.

LIEBMAN, P. A. 1975. Birefringence, dichroism and rod outer segment structure. *In* Photoreceptor Optics. A. W. Snyder and R. Menzel, editors. Springer-Verlag K G., Berlin, West Germany. 199–214.

LIEBMAN, P. A., M. W. KAPLAN, W. S. JAGGER, and F. G. BARGOOT. 1974. Membrane structure changes in rod outer segments associated with rhodopsin bleaching. *Nature (Lond.)*. **251**:31–36.

SAIBIL, H., M. CHABRE, and D. WORCESTER. 1976. Neutron diffraction studies of retinal rod outer segment membranes. *Nature (Lond.)*. **262**:266–270.

SCHWARTZ, S., J. E. CAIN, E. A. DRATZ, and J. K. BLASIE. 1975. An analysis of lamellar x-ray diffraction from disordered membrane multilayers with application to data from retinal rod outer segments. *Biophys. J.* **15**:1201–1233.

SIDMAN, R. L. 1957. The structure and concentration of solids in photoreceptor cells studied by refractometry and interference microscopy. *J. Biophys. Biochem. Cytol.* **3**:15–30.

THORNBURG, W. 1957. The form birefringence of lamellar systems containing three or more components. *J. Biophys. Biochem. Cytol.* **3**:413–419.

UHL, R., K. P. HOFMANN, and W. KREUTZ. 1977. Measurements of fast light-induced disc shrinkage within bovine rod outer segments by means of light-scattering transient. *Biochim. Biophys. Acta.* **469**:113–122.

YAEGER, M. 1975. Neutron diffraction analysis of the structure of retinal photoreceptor membranes and rhodopsin. *Brookhaven Symp. Biol.* **27**:III, 3–36.

Young, R. 1967. The renewal of photoreceptor cell outer segments. *J. Cell Biol.* **33**:61–72.